CHAPTER 107

LABORATORY INVESTIGATION ON THE STABILITY OF A SPHERICAL ARMOR UNIT OF A SUBMERGED BREAKWATER

N. MIZUTANI,[1] K. IWATA,[2] T. M. RUFIN JR.,[3] and K. KURATA[4]

Abstract

The stability of the armor unit in relation to the wave force acting on a spherical armor unit of a submerged breakwater was discussed experimentally in this paper. Stability models were derived to relate the stable weight of the spherical armor unit with the wave forces acting. The proposed models were in good agreement with the experimental results. And the vicinity around the leading crown-edge was revealed to be the most critical location of the submerged breakwater.

1. INTRODUCTION

The submerged breakwater is one type of coastal structure that can compensates the demerits of a detached breakwater in the prevention of beach erosion. In the design of submerged breakwater, stable weight of the armor unit must be properly evaluated. The critical stable weight of the armor unit depends largely on an accurate estimation of the wave forces and on a complete understanding of its generating mechanism and the wave characteristics; thus, it is necessary to estimate the stability in relation to wave forces in assessing the overall effectiveness of such structure. A number of researches has been conducted on the stability of armor units and many estimation methods have been proposed, such as Hudson (1959) and Van Der Meer (1987). Uda et al. (1989) developed an estimation method of stable weight of armor units of an artificial reef based on the laboratory experiment of armor stability. However, previous researches show that very few studies about wave force acting on armor units have been conducted; although there has been some study on wave forces acting on an armor rubble of a rubble-mound slope breakwaters (Iwata et al., 1985), still its wave force characteristics are not fully clarified. Hence, this paper aims to present experimentally the stability of a spherical armor unit of a submerged breakwater in relation to the wave forces acting on it.

[1]D. Eng., Assoc. Professor, Dept. of Civil Eng., Nagoya Univ., Nagoya 464-01, JAPAN
[2]M. ASCE, D. Eng., Professor, Dept. of Civil Eng., Nagoya Univ., Nagoya, JAPAN
[3]M. Eng., Graduate Student, Dept. of Civil Eng., Nagoya Univ., Nagoya, JAPAN
[4]D. Eng., Researcher, Toyo Construction Co. Ltd., Nishinomiya 663, JAPAN

2. EXPERIMENTAL PROCEDURE

The stability tests and the laboratory observations of wave forces acting on a spherical armor unit on a submerged breakwater were carried out using an indoor wave tank (25 m long x 0.7 m wide x 0.9 m deep). The submerged breakwater, as shown in Fig. 1, was installed on a horizontal bed. The model of the breakwater was prepared using spheres, diameter $D = 0.03$ m, to exclude complexities due to shape complexity of natural stones. The porosity of the submerged breakwater was 26%. Two separate sets of experiments under different water depths were performed in this study, hereafter to be referred to as EXPT90 and EXPT91 respectively.
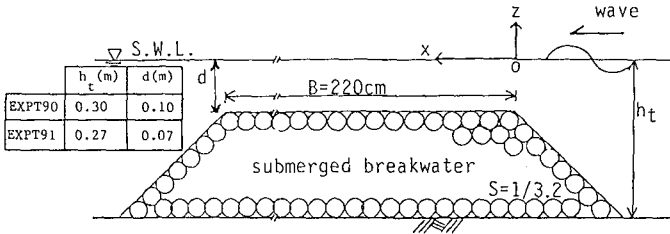

	h_t (m)	d (m)
EXPT90	0.30	0.10
EXPT91	0.27	0.07

B=220cm

submerged breakwater

S=1/3.2

Fig. 1 Schematic diagram of submerged breakwater.

2.1 Stability Measurement

Eight and 12 samples of spheres of the same diameter but varying in weight were prepared for EXPT90 and EXPT91, respectively. Regular waves with different wave periods (EXPT90: T = 1.0, 1.41, 1.60 s; EXPT91: T = 1.0, 1.4, 1.80 s) were generated in this experiment. For every designated locations on the submerged breakwater, the critical wave height of each sample in each period were determined. Critical wave height is defined as the minimum wave height required to move a given sample of sphere. The determination was made by generating series of experimental trials with different values of wave height until the critical wave height is attained. Then, the corresponding water surface elevations and horizontal and vertical water particle velocities (u and w) were measured with electric capacitance-type wave gauges and an electromagnetic-type velocimeter. For EXPT91, wave forces in horizontal and vertical directions (F_x and F_z) were also measured with cantilever-type wave force meters. Measurements were conducted for both embedded and non-

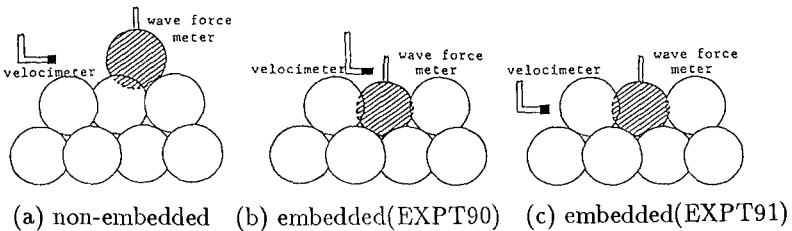(a) non-embedded   (b) embedded(EXPT90)   (c) embedded(EXPT91)

Fig. 2 Methods of wave force and velocity measurements.

embedded conditions and the methods of stability measurement for each set of experiment are given in Fig. 2. However, the half-embedded condition was adopted in EXPT90 since few movements in embedded conditions were observed.

2.2 Wave Force Measurement

Wave force measurements were also performed in this study to determine the fundamental characteristics of wave forces under a given wave conditions. Regular waves with the same periods as in the stability measurements were generated. Four different values of wave height ($H_I = 0.03, 0.05, 0.07, 0.10$ m) which include both non-breaking and breaking wave conditions were assigned in this experiment. For each wave condition, the water surface profile, horizontal and vertical water particle velocities and wave forces were measured for both non-embedded and embedded conditions using the same instruments as in the previous experiments. The methods of wave force and velocity measurement are shown in Fig. 2.

Figure 3 shows the schematic illustration of the wave force meter devised for this experiment. It consists of a supporting rod and a cantilever with a sensing sphere on its head. The cantilever was covered with shield of appropriate shape to minimize the flow-turbulent effect. The wave force acting on the sphere causes strain on the cantilever and the output signal of the strain gauge on the cantilever together with the calibration table gives the magnitude of the wave force. The natural frequencies of wave force meters are more than 10Hz, which are much higher than the incident waves but its effect on wave forces is negligible and is removed using a low pass filter. The same diameter of sensing sphere was chosen for the non-embedded condition , however, a smaller diameter, $D = 0.025$ m, of sensing sphere was used for the embedded condition in order to prevent contact with the surrounding spheres.
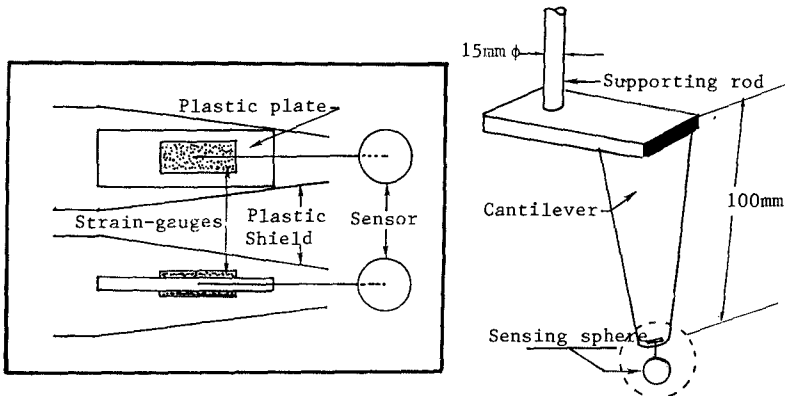

Fig. 3 Schematic diagram of cantilever-type wave force meter.

3. Stability of the Armor Unit

The relationship between the dimensionless critical stable weight of the armor unit $W'_c/\rho g D^3$ and the dimensionless maximum velocity $u_m/\sqrt{gd}$ is shown in Fig. 4, where W'_c is the critical stable weight of the armor unit in water, ρ is the density of water, g is the gravitational acceleration and subscript m indicates the maximum value. In the figure, the dimensionless maximum velocities corresponding to KC_x number equal to 10 and 20 are also indicated, where $KC_x = u_m T/D$ is the Keulegan-Carpenter number. It it shown that the dimensionless critical stable weight is proportional to the velocity when KC_x is less than 10. On the other hand, it is proportional to the maximum velocity squared for KC_x larger than 10.
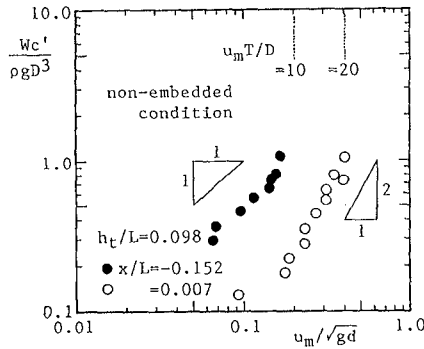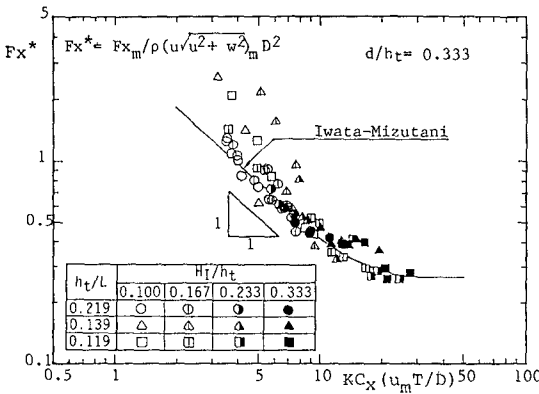

Fig. 4 Relationship between $W_c'/\rho g D^3$ and $u_m/\sqrt{gd}$.

Figure 5 shows the relationship between the dimensionless maximum wave force $Fx_m/\rho(u\sqrt{u^2 + w^2})_m D^2$ and KC_x. In the figure, the mean value obtained for an isolated sphere (Iwata and Mizutani, 1989) is also plotted. It can be observed that $Fx_m/\rho(u\sqrt{u^2 + w^2})_m D^2$ is inversely proportional to KC_x when

(a) non-embedded(EXPT90)

Fig. 5 Relationship between $Fx_m/\rho(u\sqrt{u^2 + w^2})_m D^2$ and KC_x.

$KC_x < 10$. The inclination becomes mild when $10 < KC_x < 20$ and it approaches a constant value when $KC_x > 20$. These tendencies are quite similar to those of isolated spheres. This clearly shows that the drag force is dominant over the inertia force when $KC_x > 20$; conversely, the inertia force is a significant component when $KC_x < 20$, especially when $KC_x < 10$. And this causes the difference in the inclination of variation as given in Fig. 4. Thus, it can be concluded that the inertia force is also an important force component for the stability of the armor unit. Furthermore, this result suggests that a more accurate estimation of stable weight of an armor unit will be attained if it is expressed in terms of the wave forces acting rather than by its velocity.

4. STABILITY MODEL

In all stability trials, the motion of all samples was observed to be a rotating-type. This signifies that the spherical armor units starts to move when the overturning moment overcomes the restoring moment. Thus, the relationship between the stable weight and the wave force acting is obtained from the equilibrium state of moments. The force components considered in the system are the wave forces, gravitational force, buoyant force and frictional force. However, the frictional force between spheres is not considered in the analysis; since, the contact area between spherical armor units is very small and its contribution is considered to be negligible as compared to the other forces. This treatment, however, leads to a conservative estimation in the engineering point of view. The schematic diagram of the equilibrium state is shown in Fig. 6, and the following equations are obtained from this balance of moments.

For the non-embedded condition:

$$\frac{W_c}{\rho g D^3} = \left(\frac{2\sqrt{2}}{\cos\theta - 2\sqrt{2}\sin\theta}\right)\frac{Fp_m}{\rho g D^3} + \frac{B_F}{\rho g D^3} + \frac{Fn_m}{\rho g D^3} \tag{1}$$

For the embedded condition:

$$\frac{W_c}{\rho g D^3} = \frac{Fz_m}{\rho g D^3} + \frac{B_F}{\rho g D^3} + \frac{Fx_m}{\rho g D^3}. \tag{2}$$
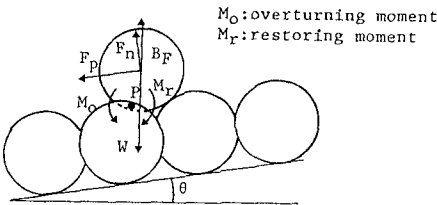
M_0: overturning moment
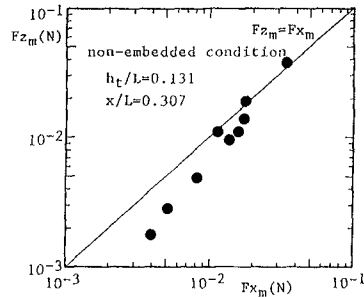M_r: restoring moment

Fig. 6 Balance of moment and force.

Fig. 7 Relationship between Fz_m and Fx_m.

where Fp_m and Fn_m are the maximum tangential and normal components of wave force, respectively, and B_F is the buoyant force.

In the given equations, the third term should be the instantaneous value when the wave force component in the first term becomes maximum. However, based on the experimental results, there are cases that the normal and tangential wave forces or vertical and horizontal wave forces attain its maximum values almost instantly. This phenomenon corresponds to the most dangerous condition of armor stability; thus, the maximum values instead of the instantaneous values are adopted in the third term of the given equations.

However, for easier evaluation of the stable weight, the given equations should be expressed in terms of one wave force component. Figure 7 shows an example of the relationship between Fz_m and Fx_m. From the figure, the orthogonal wave forces are correlated by a linear relationship as given in the following equation.

$$Fn_m = \phi Fp_m \qquad\qquad Fz_m = \phi Fx_m \qquad\qquad (3)$$

where ϕ is the coefficient determined by least square method and varies with the settlement condition (non-embedded or embedded) and location on the submerged breakwater.

Substitution of Eq.(3) into Eqs.(1) and (2) yields the final form of the stability model and are given as follows:

For the non-embedded condition:

$$\frac{W_c}{\rho g D^3} = \left(\frac{2\sqrt{2}}{\cos\theta - 2\sqrt{2}\sin\theta} + \phi\right)\frac{Fp_m}{\rho g D^3} + \frac{B_F}{\rho g D^3} \qquad\qquad (4)$$

$$\phi = 1.0$$

For the embedded condition:

$$\frac{W_c}{\rho g D^3} = \left(\frac{1+\phi}{\phi}\right)\frac{Fz_m}{\rho g D^3} + \frac{B_F}{\rho g D^3} \qquad\qquad (5)$$

$$\phi = 0.7 \text{ for armor units on the crown}$$
$$\phi = 1.6 \text{ for armor units on the slope}$$

The proposed model, hereafter to be referred as MODEL A, expresses the stable weight in terms of two wave force components together with the buoyant force. Some of previous research, however, considered only one wave force component which is in the direction of movement. This type of condition is also considered in this paper, another model without the third term of Eqs. (1) and (2) is derived as given in Eqs. (6) and (7) and hereafter to be referred as MODEL B.

For the non-embedded condition:

$$\frac{W_c}{\rho g D^3} = \frac{2\sqrt{2}}{\cos\theta - 2\sqrt{2}\sin\theta} \frac{Fp_m}{\rho g D^3} + \frac{B_F}{\rho g D^3} \tag{6}$$

For the embedded condition:

$$\frac{W_c}{\rho g D^3} = \frac{Fz_m}{\rho g D^3} + \frac{B_F}{\rho g D^3} \tag{7}$$

The comparisons between experimental results and the proposed models are given in Fig.8, from which an excellent agreement between the calculated value of MODEL A and the experimental value is revealed. On the other hand, MODEL B underestimates the stable weight as shown in Fig.8(b) and (c). This implies that the normal component of wave force for the non-embedded condition and the horizontal component for the embedded condition are both

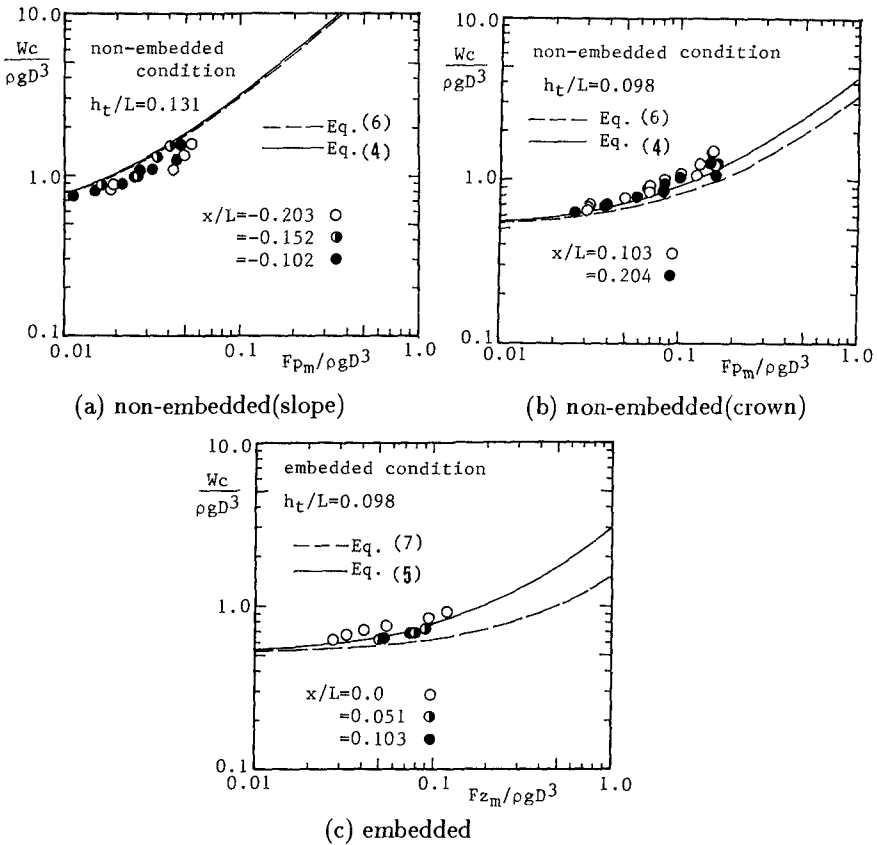(a) non-embedded(slope)

(b) non-embedded(crown)

(c) embedded

Fig. 8 Relationship of $W/\rho g D^3$ with maximum dimensionless wave force.

significant in the armor stability. The normal component of wave force enlarges the upward force, thereby, making the non-embedded armor unit more unstable. Whereas, the horizontal force enlarges the overturning moment of the embedded armor unit.

Based on these two models, it is shown that the third terms are very important in a precise estimation of the armor stability. Thus, it can be concluded that both wave force components should be taken into account for an accurate estimation of stable weight of an armor unit. Very small difference between MODEL A and MODEL B is obtained for the non-embedded armor unit on the sloping part; since, in this situation, the tangential component of wave force is dominant over the normal component.

5. Maximum Wave Force

The proposed models express the stable weight of an armor unit in terms of the maximum wave forces acting on it. Therefore, an accurate estimation of wave force is required in the evaluation of stable weight.

Figures 9 and 10 show the variations of the dimensionless maximum wave forces, $Fx_m/\rho g H D^2$ and $Fz_m/\rho g H D^2$ with dimensionless distance from the leading crown-edge, x/L, as obtained from the wave force measurement experiments, where x is the horizontal distance measured from the leading crown-edge and L is the wavelength. Regardless of h_t/L, where h_t is the still water depth at the toe of the submerged breakwater, the variations under the same H_I/h_t value are quite similar. However, different variations of $Fx_m/\rho g H D^2$ are obtained between non-breaking and breaking conditions. In Fig. 9, a typical variation of non-breaking and breaking wave conditions are shown with broken and solid lines, respectively.

For the non-embedded condition, $Fx_m/\rho g H D^2$ increases with x/L on the slope and it reaches a maximum value near $x/L = 0.0$, regardless of wave breaking. On the crown, $Fx_m/\rho g H D^2$ under breaking wave condition first decreases rapidly with increasing value of x/L, then takes a very large value when breaking waves attack the armor unit; and then finally decreases again. Under the non-breaking wave condition, $Fx_m/\rho g H D^2$ decreases gradually with x/L, but a very large value at $x/L = 0.7$ is again attained. In general, $Fx_m/\rho g H D^2$ on the crown under the non-breaking wave condition is larger than that of the breaking wave condition except in the vicinity of the crown-edge.

For embedded condition, the variation of $Fx_m/\rho g H D^2$ with x/L is smaller as compared to the non-embedded condition, because the variation of its velocity is also small.

The variation of $Fz_m/\rho g H D^2$ with x/L is shown in Fig.10; however, the values of $Fz_m/\rho g H D^2$ and its variation with x/L and H_I/h_t are smaller than those of $Fx_m/\rho g H D^2$. The quantity $Fz_m/\rho g H D^2$ for both embedded and non-embedded conditions show no significant difference in magnitude except at $x/L = 0.0$ where it becomes large under the non-embedded condition.
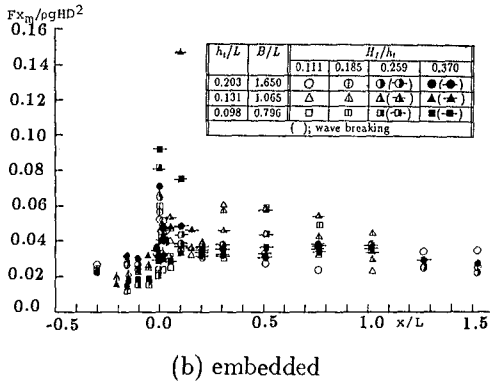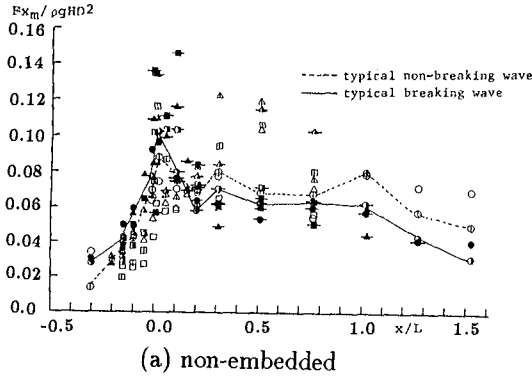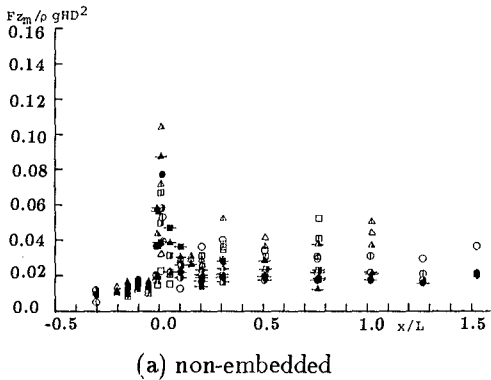
$Fx_m/\rho g H D^2$

(a) non-embedded

$Fx_m/\rho g H D^2$

h_t/L	B/L	H_t/h_t			
		0.111	0.185	0.259	0.370
0.203	1.650	◯	◑	◑(-◑-)	●(-●-)
0.131	1.065	△	◮	▲(-▲-)	▲(-▲-)
0.098	0.796	▢	◪	◪(-◪-)	◼(-◼-)
		( ); wave breaking			

(b) embedded

Fig. 9 Relationship of $Fx_m/\rho g H D^2$ with x/L.

The relative crown depth, d/h_t also has a significant effect on wave force, where d is the depth of water from the crown. Experimental results show that a smaller d/h_t results in a larger wave forces, although the figures corresponding to larger d/h_t are not shown in this paper (Iwata et al. 1991,1992, Mizutani et al., 1991, Rufin, 1992).
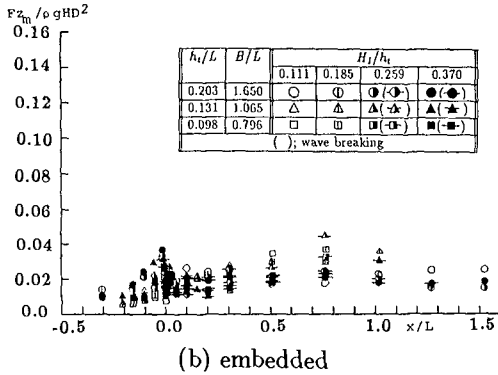
$Fz_m/\rho g H D^2$

(a) non-embedded

$Fz_m/\rho g H D^2$

h_t/L	B/L	H_I/h_t			
		0.111	0.185	0.259	0.370
0.203	1.650	O	⊕	◐(◑)	●(◉)
0.131	1.065	△	▲	▲(⊿)	▲(▲)
0.098	0.796	□	⊡	◧(◧)	■(■)
		( ); wave breaking			

(b) embedded

Fig. 10 Relationship of $Fz_m/\rho g H D^2$ with x/L.

The relative crown depth, d/h_t also has a significant effect on wave force, where d is the depth of water from the crown. Experimental results show that a smaller d/h_t results in a larger wave forces, although the figures corresponding to larger d/h_t are not shown in this paper (Iwata et al. 1991,1992, Mizutani et al., 1991, Rufin, 1992).
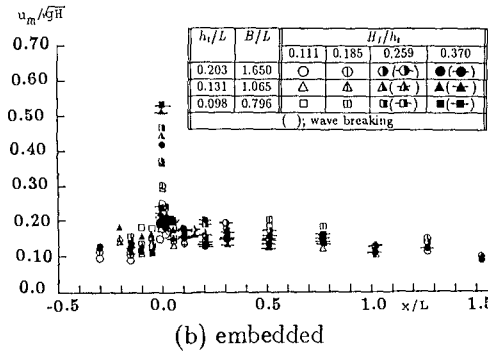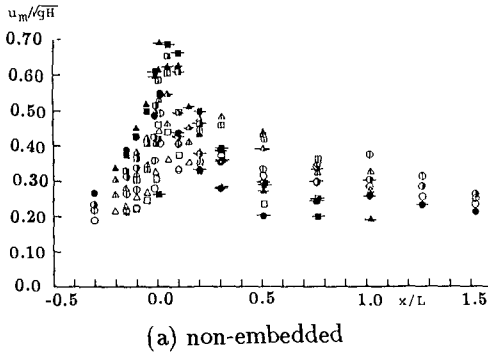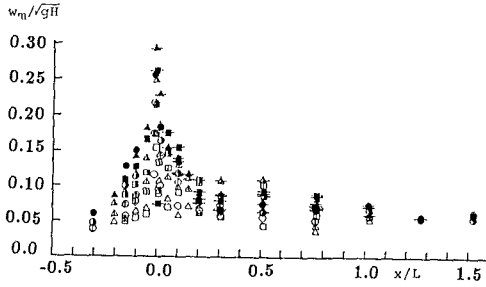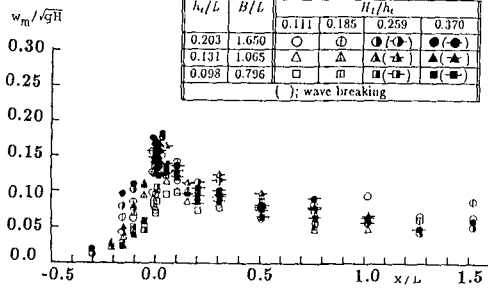
$u_m/\sqrt{gH}$

(a) non-embedded

$u_m/\sqrt{gH}$

h_t/L	B/L	H_I/h_t			
		0.111	0.185	0.259	0.370
0.203	1.650	O	⊕	◐(◑)	●(◉)
0.131	1.065	△	▲	▲(⊿)	▲(▲)
0.098	0.796	□	⊡	◧(◧)	■(■)
		( ); wave breaking			

(b) embedded

Fig. 11 Relationship of $u_m/\sqrt{gH}$ with x/L.

$w_m/\sqrt{gH}$

(a) non-embedded

$w_m/\sqrt{gH}$

| h_t/L	B/L	H_t/h_t			
		0.111	0.185	0.259	0.370
0.203	1.650	O	⊕	◑ (◖)	●(◕)
0.131	1.065	△	▲	▲(◭)	▲(◮)
0.098	0.796	□	⊡	◪(◫)	■(◧)
		( ); wave breaking			

(b) embedded

Fig. 12 Relationship of $w_m/\sqrt{gH}$ with x/L.

These characteristics of wave forces are well correlated with the water particle velocities. The variation of dimensionless maximum particle velocities $u_m/\sqrt{gH}$ and $w_m/\sqrt{gH}$ with x/L are given in Figs. 11 and 12. On the slope, the velocity becomes larger with increasing x/L, due to wave shoaling, then attains a maximum value at the crown-edge. On the crown, the dimensionless maximum velocity decreases with x/L because of energy loss due to friction in the permeable structure and also due to wave breaking. A clear difference between the non-embedded and embedded conditions is observed in the horizontal component; however, no significant difference in the vertical component is observed. With regards to the effect of d/h_t, it was revealed that the dimensionless maximum velocity increases as d/h_t decreases (Iwata et al. 1991,1992, Mizutani et al., 1991, Rufin, 1992). These tendencies are similar to the dimensionless maximum wave forces. This means that the variation of dimensionless maximum wave forces is largely attributed to the velocity characteristics.

6. STABLE WEIGHT OF SPHERICAL ARMOR UNIT

Substituting the variation of maximum wave forces into Eqs. (4) and (5), the stable weight of the armor unit along the submerged breakwater is obtained. A plot showing the variations of the dimensionless stable weight of the spherical armor unit with x/L is given in Fig. 13. The discontinuity of the distribution at the leading crown-edge of the non-embedded condition is attributed to the significant contribution of the gravitational force. On the crown, the gravitational force acts only as a restoring force; however, some part of it acts as an overturning moment on the slope.
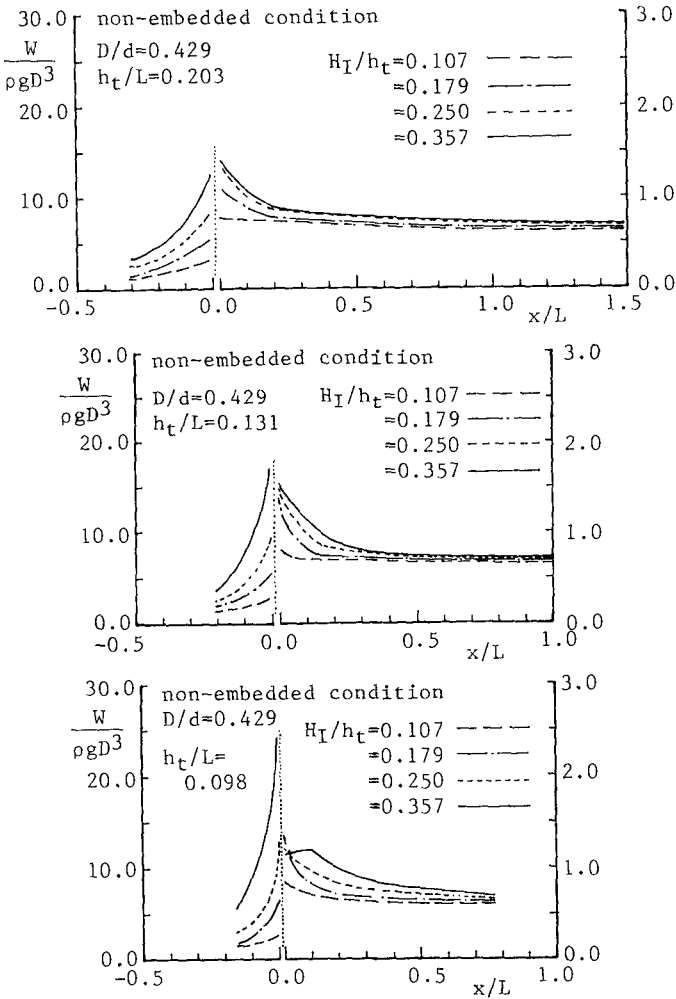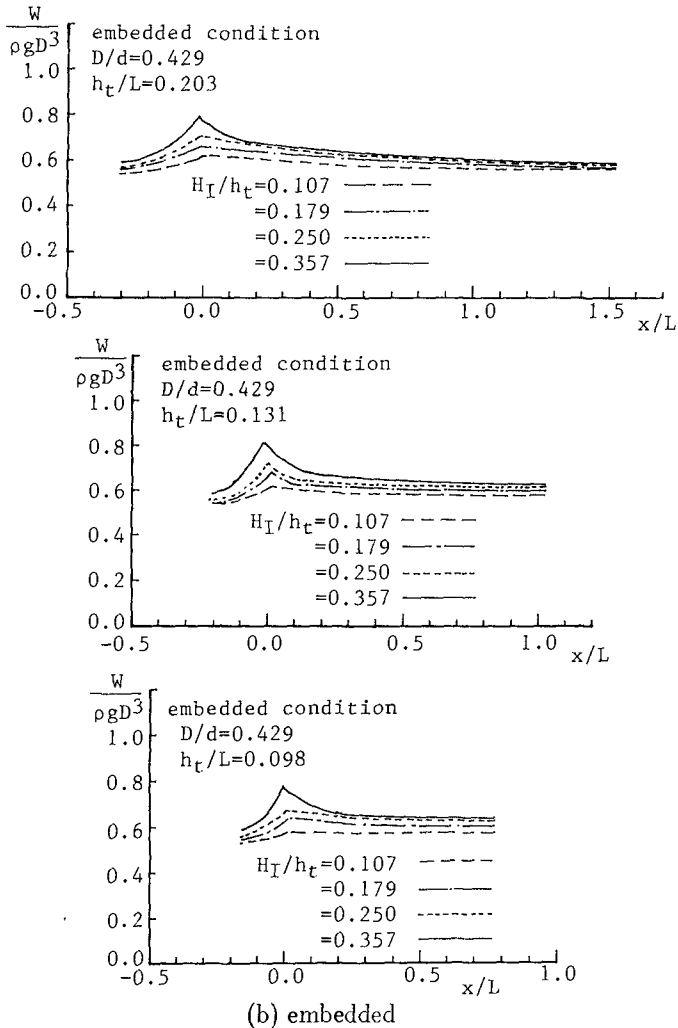

(a) non-embedded

(b) embedded

Fig. 13 Variation of $W/\rho g D^3$ with x/L.

It is confirmed from the figures that the stable weight increases with incre-
ments of wave height on the slope where wave breaking does not occur. And
the stable weight is greater around the vicinity of the crown-edge and at the
location where wave breaks or where the horizontal roller and oblique-down
vortex attack the armor units. Except at the vicinity of the crown-edge, there
is a very little difference in the stable weight of the armor unit on the crown.

7. CONCLUSION

Results obtained from this study can be summarized as follows:
(1) The vicinity around the crown-edge is revealed to be the most critical lo-

cation on the submerged breakwater.

(2) A breaking wave greatly affects the stability of armor units.

(3) Both horizontal and vertical or tangential and normal wave forces should be taken into account in the estimation of stable weight of armor units.

(4) Stability models are derived to relate the stable weight of the armor unit with the wave forces acting. Also, the variations in the stable weight of spherical armor units on the submerged breakwater are given graphically.

ACKNOWLEDGMENT

REFERENCES

[1] Hudson, R. Y.(1959): Laboratory Investigation of Rubble Mound Breakwaters, *Proc. ASCE*, Vol.85, WW3, pp.93-121.

[2] Iwata, K., N. Mizutani, T.M. Rufin Jr., N. Totsuka (1992): Laboratory Analyses on Wave Forces Acting on a Spherical Armor Unit and the Stability of the Submerged Breakwater, *Tech. Report, Toyo Const. Co. Ltd..*

[3] Iwata, K., N. Mizutani and T.M. Rufin Jr. (1991): Experimental Study on Wave Force Acting on a Spherical Unit of an Artificial Reef, *Tech. Report, Toyo Const. Co. Ltd..*

[4] Iwata K. and N. Mizutani (1989): Experimental Study on Wave Force Acting on Submerged Sphere, *Proc. 8th Int. Conf. on OMAE, ASME*, Vol.2, pp.145-152.

[5] Iwata, K., Y. Miyazaki and N. Mizutani (1985): Experimental Study of the Wave Force Acting on Armour Rubble of a Rubble-Mound Slope, *Proc. Natl. Disaster Science*, Vol.7, No.2, pp.29-41.

[6] Mizutani, N., K. Iwata, T.M. Rufin Jr. and K. Kurata (1991): Experimental Study on Wave Forces Acting on an Spherical Armor Unit of the Submerged Breakwater. *Proc. Intl. Symposium on Natural Disaster Reduction and Civil Engineering.*, pp.107-115.

[7] Rufin, T. M. Jr. (1992): Laboratory Analyses on Stability and Wave Forces Acting on a Spherical Armor Unit of a Submerged Breakwater. *Master Thesis, School of Engineering, Nagoya University.*

[8] Uda, T., T. Omata and T. Saito (1989): Design Formula for the Weight of Armor Unit for an Artificial Reef, *Proc. Coastal Eng., JSCE*, Vol.36, pp.648-652 (in Japanese).

[9] Van Der Meer, J.W. (1987): Stability of Breakwater Armor Layers- Design Formulae, *Coastal Eng.* Elsevier Sci. Pub., pp.219-239.